Journal of
Applied Crystallography

ISSN 0021-8898

Received 30 July 2008
Accepted 10 October 2008

Neutron transmission of single-crystal magnesium fluoride

J. G. Barker,[a]* D. F. R. Mildner,[a] J. A. Rodriguez[a,b] and P. Thiyagarajan[c]

[a]National Institute of Standards and Technology, Gaithersburg, MD 20899, USA, [b]Department of Materials Science and Engineering, University of Maryland, College Park, MD 20740, USA, and [c]Intense Pulsed Neutron Source, Argonne National Laboratory, IL 60439, USA. Correspondence e-mail: john.barker@nist.gov

The neutron attenuation through single-crystal magnesium fluoride has been measured as a function of wavelength at both room temperature and 77 K. These data confirm a total cross section that is lower than that of MgO for wavelengths greater than 0.2 nm. MgF_2 cooled to 77 K is a slightly better filter of epithermal neutrons than MgO for obtaining a thermal neutron beam.

1. Introduction

The use of long-wavelength neutrons at reactor and pulsed sources often requires a filter for the removal of unwanted epithermal neutrons. For instruments that only require neutrons having wavelength $\lambda \geq 0.41$ nm, the polycrystalline beryllium filter provides the best performance and is commonly used. For shorter wavelengths in the thermal neutron range, strong attenuation from Bragg scattering occurs in polycrystalline materials since the Bragg condition may be satisfied over a continuous range of short wavelengths, whereas perfect single crystals eliminate the coherent Bragg scattering for all but a few narrow wavelength ranges that satisfy the Bragg condition for the particular crystal orientation. Other materials that can be produced economically as low-mosaic-spread and high-purity (> 99.99%) single crystals are routinely used as filters for these thermal neutron applications (Holmryd & Connor, 1969; Nieman *et al.*, 1980; Freund, 1983). Single-crystal filters of sapphire (Al_2O_3) at room temperature (Mildner & Lamaze, 1998), or silicon (Freund *et al.*, 1985) and magnesium oxide (Thiyagarajan *et al.*, 1998) at cryogenic temperatures, are frequently used. Table 1 lists the cross sections for all the relevant elements involved, taken from Sears (1986, 1992).

Here we consider the potential of single-crystal magnesium fluoride. IR optical-quality single-crystal MgF_2 is preferred to vitreous silica or single-crystal quartz for neutron optics experiments involving lenses (Eskildsen *et al.*, 1998; Choi *et al.*, 2000) because of its purity and greatly reduced microstructure. This results in high transmission with very little small-angle neutron scattering (SANS). To keep the absorption from impurities at less than 10% of that caused by Mg (for which the absorption cross section is only 0.063 b), the total impurity content must usually be less than 0.01 at%, with much lower levels for three highly absorbing elements (B < 2.6×10^{-4}%, Cd < 8×10^{-5}% and Gd < 4×10^{-6}%). The absorption is low and the coherent scattering length is relatively high, with low incoherent scattering, so that MgF_2 should also make a reasonable thermal neutron filter of epithermal neutrons.

2. Model calculations

Neglecting incoherent and Bragg scattering, the total macroscopic cross section $\Sigma_{\rm tot}$ as a function of temperature T can be separated into three attenuation processes: (1) temperature-independent absorption by the nuclei, (2) single-phonon scattering and (3) multiple-phonon scattering, *i.e.*

$$\Sigma_{\rm tot}(\lambda, T) = \Sigma_{\rm abs}(\lambda) + \Sigma_{\rm sph}(\lambda, T) + \Sigma_{\rm mph}(\lambda, T). \quad (1)$$

The absorption cross section is related to wavelength by

$$\Sigma_{\rm abs} = A_{\rm abs}\lambda = N(\sigma_{\rm abs}/\lambda_0)\lambda, \quad (2)$$

where N is the number of molecules per unit volume of material and $\sigma_{\rm abs}$ is the thermal absorption cross section per molecule at the standard tabulation wavelength λ_0 = 0.1798 nm. For pure MgF_2, $N = 3.07$ b^{-1} m^{-1} and $\sigma_{\rm abs} = 0.082$ b at λ_0, so that $A_{\rm abs} = 1.405$ m^{-1} nm^{-1}.

Steyerl (1977) has given an expression for the calculation of the temperature-dependent single-phonon scattering as a function of temperature T as

$$\Sigma_{\rm sph}(\lambda, T) = A_{\rm sph}\lambda = (3N\sigma_{\rm b}/M)(2m_{\rm n}k\Theta_{\rm D}/h^2)^{1/2}\lambda \times \sum_{n=0} B_n x^{n-1}/[n!(n+2.5)], \quad (3)$$

valid for $x \leq 6$, where $x = \Theta_{\rm D}/T$. [Note that for $x > 6$ the summation in equation (3) is replaced by $3.3x^{-7/2}$.] Here $\Theta_{\rm D}$ is the Debye temperature and T is the physical temperature of the material in Kelvin, k is the Boltzmann constant, $m_{\rm n}$ is the neutron mass, h is Planck's constant, and B_n are the Bernoulli numbers. M is the bound-atom cross-section-weighted harmonic mean atomic mass number. For MgF_2, M is calculated using the expression $M^{-1} = (\sigma_{\rm Mg}/M_{\rm Mg} + 2\sigma_{\rm F}/M_{\rm F})/(\sigma_{\rm Mg} + 2\sigma_{\rm F})$, where $M_{\rm Mg}$ and $M_{\rm F}$ are the atomic mass numbers, and $\sigma_{\rm Mg}$ and $\sigma_{\rm F}$ are the bound-atom cross sections for magnesium

Table 1
A comparison of the bound coherent scattering lengths and the various cross sections of the elements found in Be, Al_2O_3, MgO, MgF_2 and SiO_2, obtained from Sears (1986, 1992).

Bound coherent scattering length: b_c; total bound scattering cross section: σ_s; bound incoherent scattering cross section: σ_i; thermal absorption cross section: σ_{abs} (at $\lambda = 0.1798$ nm). The elements are listed in order of increasing atomic absorption cross section σ_a. The error bars within parentheses represent $\pm 1\sigma$.

Element	b_c (fm)	σ_s (b)	σ_i (b)	σ_{abs} (b)
O	5.803 (4)	4.232 (6)	0.000 (8)	0.00019 (2)
Be	7.79(1)	7.63(2)	0.0018(9)	0.0076(8)
F	5.654 (10)	4.018 (14)	0.0008 (2)	0.0096 (5)
Mg	5.375 (4)	3.71 (4)	0.08 (6)	0.063 (3)
Si	4.149 (1)	2.167 (8)	0.004 (8)	0.171 (3)
Al	3.449 (5)	1.503 (4)	0.0082 (6)	0.231 (3)

and fluorine, respectively. Hence, $M = 20.41$ and the bound-atom cross section $\sigma_b = \sigma_{Mg} + 2\sigma_F = 11.75$ (5) b. The recommended Debye temperature for MgF_2 is 610 K (Kim, 2005), calculated from room-temperature elastic stiffness coefficients, in approximate agreement with the value of 626 K (Jones, 1977) deduced from acoustic measurements. [Note that Freund (1983) has given a value of $\Theta_D = 440$ K, without reference]. This results in single-phonon scattering of $A_{sph} = 3.66\ m^{-1}\ nm^{-1}$ at 293 K and $0.100\ m^{-1}\ nm^{-1}$ at 77 K. Equation (3) shows that the single-phonon cross section increases as $T^{7/2}$ at low temperatures and increases linearly with T above room temperature.

The multiple-phonon scattering that dominates at short wavelengths has been modeled as (Freund, 1983)

$$\Sigma_{mph}(\lambda, T) = \Sigma_{fa}\left\{1 - \exp\left[-(B_0 + B_T)\left\langle \sin^2(\theta/2)\right\rangle/\lambda^2\right]\right\}, \quad (4)$$

where θ is the scattering angle. The average quantity $\langle \sin^2(\theta/2)\rangle = 1/2 - 1/(3M)$, which for MgF_2 is 0.48. The free-atom macroscopic scattering cross section $\Sigma_{fa} = N[M_{Mg}^2/(M_{Mg} + 1)^2\sigma_{Mg} + 2M_F^2/(M_F + 1)^2\sigma_F] = 32.8$ (2) m^{-1}. The temperature-independent quantity $B_0 = 3h^2/(2k\Theta_D M m_p)$, where m_p is the proton rest mass, corresponds to zero-point motion and is numerically equal to $2.29 \times 10^{-3}\ nm^2$. The temperature-dependent term is given by

$$B_T = (4B_0T^2/\Theta_D^2)\int_0^{\Theta_D/T} z\,dz/[\exp(z) - 1]. \quad (5)$$

For $\Theta_D/T < 2\pi$, $B_T = 6h^2/(Mm_p)(kT)/(k\Theta_D)^2\sum_{n=0}B_n(\Theta_D/T)^n/(n+1)!$ and is equal to $2.62 \times 10^{-3}\ nm^2$ at 293 K. At 77 K, $B_T = 0.24 \times 10^{-3}\ nm^2$. The Debye–Waller factor increases as T^2 at low temperatures and increases linearly with T above room temperature. Note that Scharenberg (1972) has given a slightly different form for the multiple-phonon cross section:

$$\Sigma_{mph} = \Sigma_{fa}\left[1 - \frac{\lambda^2}{2B}\left(1 - \exp\frac{-2B}{\lambda^2}\right)\right], \quad (6)$$

where the Debye–Waller factor is $B = B_0 + B_T$. Both this form and equation (4) reduce to the same expression to first order.

3. Transmission measurements

Neutron transmission measurements have been performed with both monochromated beams and pulsed white beams using time-of-flight spectrometry. The measurements used different combinations of six right-angle prisms of optical-quality MgF_2 with sides of 25.4 mm and a width of 25.4 mm purchased from ISP Optics of Irvington, NY. The prisms were initially procured to compensate for chromatic aberrations caused by gravity in SANS measurements (Forgan & Cubitt, 1998). The crystal purity is unknown. The MgF_2 crystal has the rutile (TiO_2) structure, which exhibits tetragonal symmetry with $a_0 = 0.4623$, $c_0 = 0.3052$ nm. No special crystal orientation is specified for the prisms. For our purposes the orientation is unimportant because the single crystals have such narrow mosaic spread. Consequently the Bragg dips are very narrow in wavelength range.

All transmission measurements were taken with and without prisms, and in a sample container when cooled. The prisms were stacked in various arrangements, an example of which is shown in Fig. 1, to produce a total length of 107.8 mm. The transmission $T(\lambda)$ is determined from the ratio of the unscattered beam intensity with and without prisms, normalized by a beam monitor. The wavelength-dependent total macroscopic scattering cross section $\Sigma_{tot}(\lambda)$ for the filter is determined from $T(\lambda) = \exp[-\Sigma_{tot}(\lambda)\,l]$, where l is the length of the filter in the beam.

The first set of measurements were made using the NG3 30 m SANS instrument (Glinka *et al.*, 1998) at the NCNR (NIST Center for Neutron Research) at room temperature, $T =$ 293 (2) K, over the wavelength range $0.5 \leq \lambda \leq 2.0$ nm. The helical velocity selector produces a triangular-shaped distribution with a full width at half-maximum $\Delta\lambda/\lambda = 15\%$. A further measurement was made on the perfect crystal diffractometer (Barker *et al.*, 2005) with $\lambda = 0.24$ nm and $\Delta\lambda/\lambda = 6\%$.

Transmission measurements using the same six prisms, but now placed within a cryostat cooled with liquid nitrogen and with aluminium windows, were taken on an 8 m SANS instrument at the NCNR with $\Delta\lambda/\lambda = 15\%$, at both room temperature and 77 K. For these measurements the incident beam direction was normal to the sides of constant thickness of the six prisms for a total length of 152.4 mm. There was no special grinding needed on the sides of the prisms.

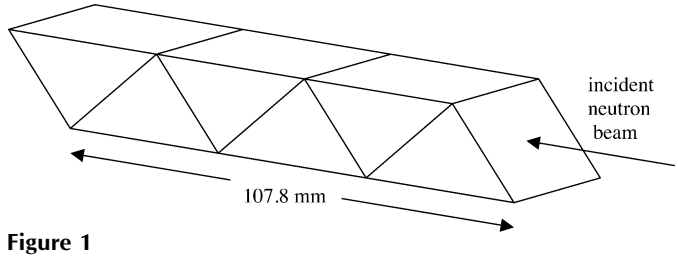

Figure 1
The arrangement of the six prisms for the initial measurements on the NG7 SANS spectrometer, to form a block of constant thickness $t =$ 107.8 mm. The prisms were arranged in different ways for the other measurements, as indicated in the text.

Additional room-temperature transmission measurements were performed on the time-of-flight small-angle neutron diffractometer (SAND; Thiyagarajan *et al.*, 1997) at the Intense Pulsed Neutron Source (IPNS) at Argonne National Laboratory, in order to extend the wavelength range into the thermal neutron region with $\lambda < 0.5$ nm and particularly into the region of minimum attenuation. Details of such measurements are given by Mildner & Lamaze (1998). The incident beam was normal to the sides of constant thickness for five prisms with a total length of 127.0 mm, such that the transmission was between 0.4 and 0.7 for the wavelength range $0.15 < \lambda < 1.2$ nm, but significantly less than 0.4 for $\lambda < 0.15$ nm. The wavelength resolution after rebinning of data was $\Delta\lambda/\lambda \leq 5\%$.

Further transmission measurements were made on the time-of-flight Disk Chopper Spectrometer (DCS; Copley & Cook, 2003) at the NCNR to extend the $T = 77$ K measurements into the thermal neutron region range $0.1 < \lambda < 1.5$ nm, with $\Delta\lambda = 0.03$ nm after rebinning of data. The sample thickness was 107.8 mm, and a close cycle refrigerator was used to control the temperature.

Finally, transmission measurements were made on the NG7 30 m SANS instrument at the NCNR using four prisms stacked to produce a 50.8 mm length in the beam over the wavelength range $0.6 \leq \lambda \leq 2.0$ nm, with $\Delta\lambda/\lambda = 15\%$. Transmissions were measured at three separate temperatures of 293, 373 and 523 K.

Fig. 2 shows the attenuation results as a function of wavelength at both room temperature and 77 K. Dips in the transmission caused by Bragg reflections were not observed in MgF_2, indicating that the crystalline mosaic spread is sufficiently small. The linear dependence at long wavelengths accounts for both the absorption (independent of temperature) and the single-phonon scattering, which is temperature dependent and may be reduced by cryogenic means. Linear fits to the data having $\lambda \geq 0.8$ nm indicate an attenuation of 6.32 m^{-1} nm^{-1} at room temperature and 1.49 m^{-1} nm^{-1} at 77 K. The data indicate that most of the phonon scattering present in the 293 K data has been eliminated at 77 K.

4. Analysis

The data were fitted to a curve of the form

$$\Sigma_{\rm tot}(\lambda, T) = A\lambda + \Sigma_{\rm fa}\{1 - \exp[-(B/\lambda^2 + D/\lambda^4)]\}, \quad (7)$$

which accounts for both the linear attenuation at long wavelengths for absorption and single-phonon scattering, and the multiple-phonon scattering at short wavelengths. The additional term D was originally introduced by Carpenter *et al.* (1989) to account for anharmonic effects in the Debye–Waller factor to improve the quality of the fit.

Fig. 3 shows the total cross sections determined from all the measurements normalized by the wavelength λ. The long-wavelength-independent asymptotic values of A appear as horizontal lines in the figure. From these data we obtain A = 6.32 (13) m^{-1} nm^{-1} at $T = 293$ K, and A = 1.49 (7) m^{-1} nm^{-1} at $T = 77$ K. Using only data for $\lambda \geq 0.8$ nm obtained at four different temperatures, we show the experimental values for A in Fig. 4 as symbols, together with the calculated values $A = A_{\rm abs} + A_{\rm sph}$ obtained using equations (2) and (3) with $\Theta_{\rm D}$ = 610 K as a dashed line. The observed values for A at the higher temperatures considerably exceed the calculation (A = 5.06 m^{-1} nm^{-1} at $T = 293$ K). Better agreement between the

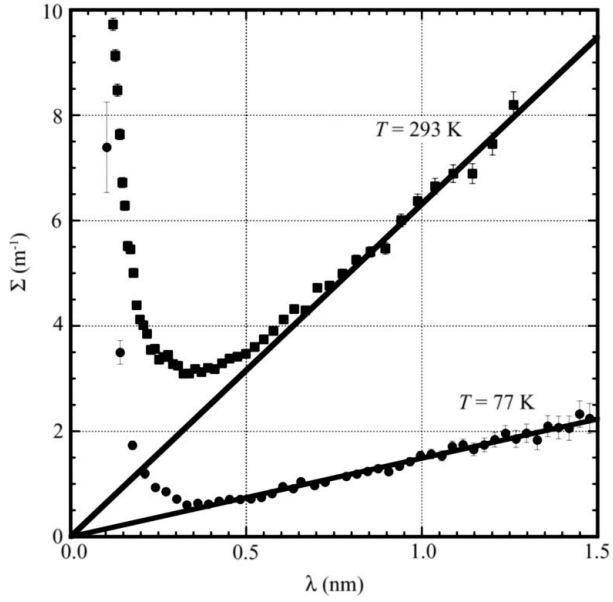

Figure 2
The attenuation coefficients for single-crystal MgF_2 measured by time-of-flight at ambient temperature $T = 293$ K using the SAND instrument at IPNS (squares), and at $T = 77$ K using the DCS instrument at the NCNR (circles). The straight lines are fits to data having $\lambda \geq 0.8$ nm according to equation (7). The error bars represent $\pm 1\sigma$.

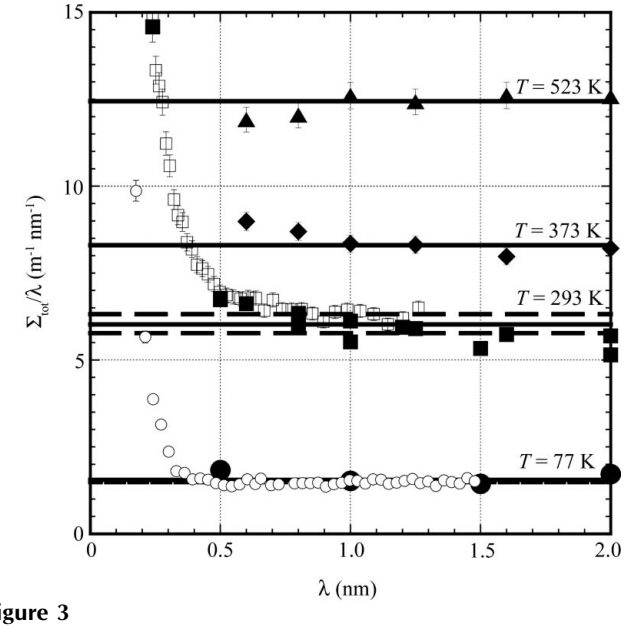

Figure 3
The total cross section $\Sigma_{\rm tot}$ normalized by wavelength λ. Open symbols are from time-of-flight measurements and closed symbols are from monochromatic beam measurements. The horizontal lines are average values obtained for data having $\lambda \geq 0.8$ nm. The three separate lines at $T = 293$ K were obtained by fitting data from each measurement separately.

Table 2
A compilation of material parameters for several different filter materials.

The order of materials is arranged from best to worst figure-of-merit ratio R at $T = 0$ K according to equation (7). References for Debye temperatures are given in the text.

Material	N (b^{-1} m^{-1})	M (u)	A_{abs} (m^{-1} nm^{-1})	θ_D (K)	Σ_{fa} (m^{-1})	λ_{min} (nm)	$R(\lambda_{min})$
Be	12.35 (1)	9.0122 (1)	0.52 (5)	1481 (16)	76.3 (2)	0.68 (2)	0.0070 (5)
MgO	5.357 (2)	19.04 (1)	1.88 (9)	938	38.4 (2)	0.32 (1)	0.023 (1)
MgF_2	3.071 (3)	20.405 (5)	1.40 (7)	610	32.8 (2)	0.38 (1)	0.024 (1)
SiO_2	2.66 (1)	17.538 (3)	2.54 (4)	580 (20)	25.31 (5)	0.304 (2)	0.0456 (7)
Al_2O_3	2.345 (6)	17.351 (2)	6.05 (8)	1032	32.99 (5)	0.206 (2)	0.0565 (6)
Si	4.9939 (2)	28.086 (1)	4.76 (8)	543 (8)	10.10 (4)	0.158 (1)	0.112 (1)

experimental values and the calculated curve is obtained using a lower temperature of 520 (20) K, shown as a solid line, rather than the recommended Debye temperature of 610 K. The discrepancy between the fitted and recommended Debye temperatures is likely caused by simplifying assumptions incorporated into equation (3) when applying the Debye model in the experimental temperature range.

Fig. 5 shows the time-of-flight data obtained at room temperature on the SAND instrument (squares) and at T = 77 K on the DCS instrument (circles). The solid lines are fits of B and D using equation (7), employing the previous values of A for the linear term. The dashed curves use equation (4) with Θ_D = 520 K to determine B, with $D = 0$.

5. Comparison with other filters

We now compare MgF_2 with the other single-crystal filters. The filter preferentially attenuates unwanted epithermal neutrons with wavelengths less than 0.02 nm, while transmitting the thermal and cold neutron wavelengths used by the instrument. Nieman *et al.* (1980) have defined a figure of merit (FOM) for filters as a ratio of cross sections, $R(\lambda) = \Sigma_{tot}(\lambda)/\Sigma_{fa}$, the attenuation at the instrument wavelength λ relative to the attenuation of epithermal neutrons, with the best epithermal filter material having the lowest FOM.

Using the Freund model at $T = 0$, with $\langle \sin^2(\theta/2) \rangle = 1/2$, it can be shown that the ratio R has a minimum at the wavelength

$$\lambda_{min} \cong \left(\frac{\Sigma_{fa} B_0}{A_{abs}}\right)^{1/3} \propto \left(\frac{\Sigma_{fa}}{A_{abs} M \Theta_D}\right)^{1/3}, \quad (8)$$

which occurs at λ = 0.38 nm for MgF_2, with a minimum value of

$$R(\lambda_{min}) \cong \frac{3}{2}\left(\frac{A_{abs}^2 B_0}{\Sigma_{fa}^2}\right)^{1/3} \propto \left(\frac{A_{abs}^2}{\Sigma_{fa}^2 M \Theta_D}\right)^{1/3}. \quad (9)$$

We compare the calculated cross sections at $T = 0$ K for single-crystal Be, MgF_2, MgO, SiO_2, Al_2O_3 and Si as a neutron filter. Table 2 gives the relevant material parameters for the calculation of the figure-of-merit ratio R and the value of λ_{min} for the chosen filter materials. The figure-of-merit favors heavy atoms with large Debye temperature and large free-atom cross section. Despite being light, single-crystal beryllium would be best, if it were available, though the minimum in the cross section occurs at longer wavelengths. The absorption cross section in both MgO and MgF_2 is dominated by magnesium and both materials have approximately the same figure-of-

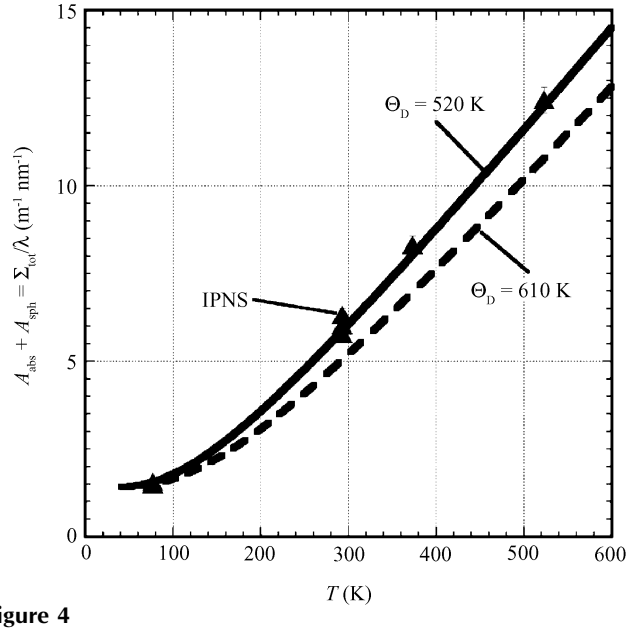

Figure 4
The mean value for the measured total cross section normalized by wavelength for all data having $\lambda \geq 0.8$ nm obtained at four different temperatures. The curves show the sum of the single-phonon and the absorption cross section $(\Sigma_{abs} + \Sigma_{sph})/\lambda = A_{abs} + A_{sph}$, calculated assuming a Debye temperature, Θ_D, of 610 K for the dashed curve and 520 K for the solid curve.

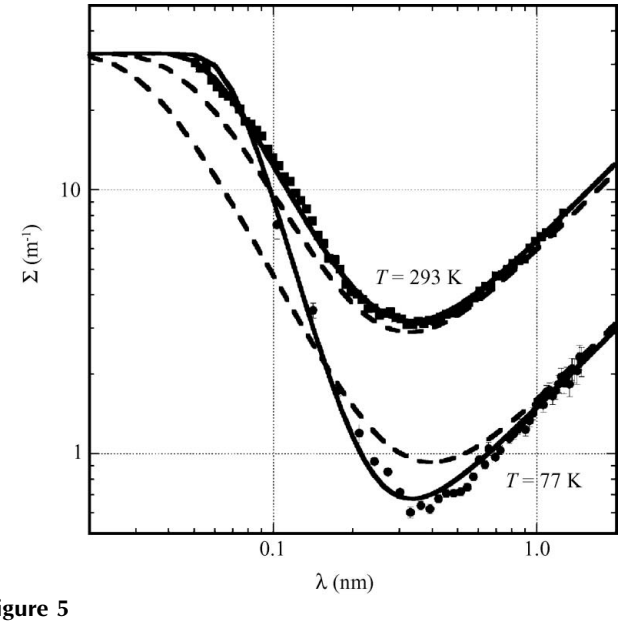

Figure 5
The attenuation coefficient for single-crystal MgF_2 measured by time-of-flight at ambient temperature T = 293 K at IPNS (squares), and at T = 77 K using the DCS instrument at the NCNR (circles). The solid curves use fits to determine A, B and D as shown in Table 3. The dashed curves assume $D = 0$, with A estimated from equations (2) and (3) and B estimated according to equation (5) with Θ_D = 520 K.

merit. Since the atomic fraction of magnesium is a third less in MgF_2 than in MgO, the absorption per molecule will be a third lower. However, this is largely compensated by MgF_2 having a Debye temperature approximately a third lower than MgO.

The Debye temperature Θ_D for a given material is often found to differ somewhat depending on the specific measurement and temperature. The values of Θ_D for the materials in Table 2 are those obtained from Ahlers (1966) for Be, Striefler & Barsch (1975) for SiO_2 and Batterman & Chipman (1962) for Si, whereas the values for Al_2O_3 and MgO are those used by Mildner & Lamaze (1998) and Thiyagarajan *et al.* (1998). Freund (1983) has also given values for Debye temperature for many filter materials, typically lower than the above reference values.

Fig. 6 shows the fitted curves of the figure-of-merit R of four different filter materials (Si, Al_2O_3, MgO and MgF_2) as a function of wavelength. Table 3 gives the fit parameters used for these curves; the values for MgF_2 are from this article, while those for Al_2O_3 are from Mildner & Lamaze (1998), those for MgO are from Thiyagarajan *et al.* (1998) and those for Si are from Freund *et al.* (1985). High-quality single-crystal silicon is the cheapest material but gives the poorest performance owing to the much higher atomic absorption cross section of Si. The next cheapest material to obtain in suitable quality is sapphire, Al_2O_3. The rather high Debye temperature allows this material to be used at room temperature with performance nearly twice as good as that of cooled silicon. MgO and MgF_2 when cooled both show much better performance than sapphire. Both materials cost more than sapphire but are readily available in suitable quality. MgO single crystals are often used as substrates for growing thin films. High-quality MgF_2 is used in refractive optics with infrared radiation but the price may be high. A very large volume (300 mm diameter with 100 mm thickness) oriented MgF_2 single crystal of optical grade costs \$0.07 mm^{-3}, and even for 25 smaller crystals cut to fill the same volume from 96 mm-diameter boules the price is \$0.05 mm^{-3}. On the basis of the high Debye temperature of 938 K, the value of A for MgO should be dominated by absorption at $T = 77$ K, but the experimental fit parameter found in Table 3 is 40% larger. It is possible that impurity elements in the MgO used by Thiyagarajan *et al.* (1998) increased the long-wavelength cross section *via* increased absorption. The purity of the MgO crystals is known to be greater than 99.99 at% allowing only 0.01% of impurity. To produce the observed 40% increase in A observed by Thiyagarajan *et al.* by impurities would require 0.001 at% of boron impurity, for example.

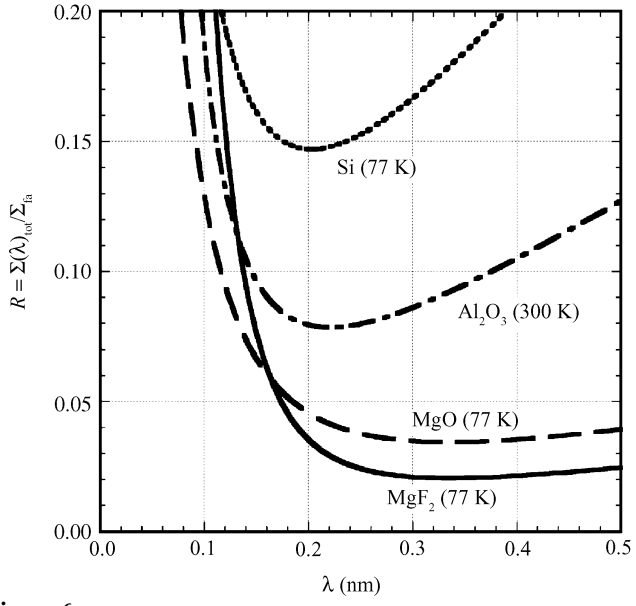

Figure 6
The relative figure-of-merit $R = \Sigma_{tot}(\lambda)/\Sigma_{fa}$ as a function of wavelength for four single-crystals filters. The parameters used in the fits are shown in Table 3; the values for MgF_2 are from this article, while those for Al_2O_3 are from Mildner & Lamaze (1998), those for MgO are from Thiyagarajan *et al.* (1998) and those for Si are from Freund *et al.* (1985).

Table 3
The fit parameters used to create Fig. 6.

The parameters were obtained from Freund *et al.* (1985) for Si, from Mildner & Lamaze (1998) for Al_2O_3 and from Thiyagarajan *et al.* (1998) for MgO. Parameters for MgF_2 were obtained from this article.

Material	T (K)	A (m^{-1} nm^{-1})	Σ_{fa} (m^{-1})	B (10^{-3} nm^2)	D (10^{-5} nm^4)
Si	77	4.83	10.10 (4)	2.11	0
Al_2O_3	300	8.11 (6)	21.2 (4)†	1.61 (8)	1.29 (10)
MgO	77	2.62 (24)	38.4 (2)	1.3 (1)	0
MgF_2	77	1.49 (7)	32.8 (2)	0.35 (6)	2.85 (15)
MgF_2	293	6.32 (13)	32.8 (2)	3.68 (10)	0.72 (6)

† Data were allowed to differ from the calculated values shown in Table 2.

6. Conclusions

We have measured the neutron attenuation of single-crystal magnesium fluoride as a function of wavelength at both room temperature and 77 K, and also as high as 523 K. The data confirm a total cross section for MgF_2 cooled to $T = 77$ K that is lower than that of MgO for wavelengths greater than 0.2 nm, making it a slightly better filter of epithermal neutrons for obtaining a thermal neutron beam. Theoretical calculations show that MgO and MgF_2 should give very similar low-temperature performance. We find that the performance of single-crystal MgF_2 at $T = 77$ K for $\lambda \geq 0.2$ nm is up to 30% better than that of MgO.

We conclude that if it is necessary to install a cryogenic MgO filter on a beamline in order to obtain lower attenuation at longer wavelengths, it is worth considering the use of single-crystal MgF_2 instead. MgF_2 is frequently used in infrared optic applications and is readily available in large single-crystal blocks.

The trade names identified in this paper do not imply recommendation or endorsement by the National Institute of Standards and Technology, nor do they imply that they are necessarily the best available for the purpose.

We thank Denis Wozniak for his assistance in the SAND experiments at IPNS funded by the US Department of Energy, BES, under contract No. DE-AC02-06CH11357 to UChicago

Argonne, LLC, and Juscelino Leao and John Copley on DCS at the NCNR for aid in setting up the close cycle refrigerator and data analysis. The elements of this work utilizing the DCS, PCD and NG3 30 m SANS instruments at the NCNR are supported in part by the National Science Foundation under agreement No. DMR-0454672.

References

Ahlers, G. (1966). *Phys. Rev.* **145**, 419–423.
Barker, J. G., Glinka, C. J., Moyer, J. J., Kim, M. H., Drews, A. R. & Agamalian, M. (2005). *J. Appl. Cryst.* **38**, 1004–1011.
Batterman, B. & Chipman, D. R. (1962). *Phys. Rev.* **127**, 690–693.
Carpenter, J. M., Mildner, D. F. R., Cudrnak, S. S. & Hilleke, R. O. (1989). *Nucl. Instrum. Methods Phys. Res. Sect. A*, **278**, 397–401.
Choi, S.-M., Barker, J. G., Glinka, C. J., Cheng, Y. T. & Gammel, P. L. (2000). *J. Appl. Cryst.* **33**, 793–796.
Copley, J. R. D. & Cook, J. C. (2003). *Chem. Phys.* **292**, 477–485.
Eskildsen, M. R., Gammel, P. L., Issacs, E. D., Detlefs, C., Mortensen, K. & Bishop, D. J. (1998). *Nature* (*London*), **391**, 563–566.
Forgan, E. M. & Cubitt, R. (1998). *Neutron News*, **9**, 25–31.
Freund, A. K. (1983). *Nucl. Instrum. Methods Phys. Res.* **213**, 495–501.
Freund, A. K., Friedrich, H., Nistler, W. & Scherm, R. (1985). *Nucl. Instrum. Methods Phys. Res. Sect. A*, **234**, 116–121.
Glinka, C. J., Barker, J. G., Hammouda, B., Krueger, S., Moyer, J. J. & Orts, W. J. (1998). *J. Appl. Cryst.* **31**, 430–445.
Holmryd, S. & Connor, D. (1969). *Rev. Sci. Instrum.* **40**, 49–56.
Jones, L. E. A. (1977). *Phys. Chem. Minerals*, **1**, 179–197.
Kim, S. (2005). Private communication.
Mildner, D. F. R. & Lamaze, G. P. (1998). *J. Appl. Cryst.* **31**, 835–840.
Nieman, H. F., Tennant, D. C. & Dolling, G. (1980). *Rev. Sci. Instrum.* **51**, 1299–1303.
Scharenberg, W. (1972). Report Jül-875-RX. Kernforschungsanlage Jülich, Germany.
Sears, V. F. (1986). *Methods of Experimental Physics*, Vol. 23, *Neutron Scattering*, part A, pp. 521–550, edited by K. Sköld & D. L. Price. New York: Academic Press.
Sears, V. F. (1992). *Neutron News*, **3**, 26–37.
Steyerl, A. (1977). *Neutron Physics*, Springer Tracts on Modern Physics, Vol. 80, pp. 57–130. Berlin, Heidelberg: Springer.
Striefler, M. E. & Barsch, G. R. (1975). *Phys. Rev. B*, **12**, 4553–4566.
Thiyagarajan, P., Epperson, J. E., Crawford, R. K., Carpenter, J. M., Klippert, T. E. & Wozniak, D. G. (1997). *J. Appl. Cryst.* **30**, 280–293.
Thiyagarajan, P., Crawford, R. K. & Mildner, D. F. R. (1998). *J. Appl. Cryst.* **31**, 841–844.